Available online at www.sciencedirect.com
ScienceDirect
Journal of Power Sources 159 (2006) 956–967
JOURNAL OF POWER SOURCES
www.elsevier.com/locate/jpowsour

Reduced-order transient thermal modeling for SOFC heating and cooling

David L. Damm, Andrei G. Fedorov *

Multiscale Integrated Thermofluidics Research Lab, GWW School of Mechanical Engineering, Georgia Institute of Technology, Atlanta, GA 30332-0405, USA

Received 18 October 2005; received in revised form 21 November 2005; accepted 23 November 2005
Available online 6 January 2006

Abstract

Transient thermal analysis plays a central role in the design and optimization of high temperature solid oxide fuel cells (SOFCs) during startup/shutdown, because of the potential for damaging thermal gradients to develop within the SOFC components. The optimal design of a heating/cooling process is one that minimizes the total time required to reach a prescribed final operating temperature, while not exceeding given thresholds of maximum allowable temperature gradients. To this end, we consider the SOFC unit cell, which is heated by hot air supplied into the oxidizer channel at a specified, time-dependent inlet temperature. Beginning with a general thermal model of the cell, we develop and evaluate limiting cases that allow closed-form analytical solutions of the time-varying temperature fields, from which heating time and maximum temperature gradient are calculated. The results are generalized by presentation in terms of a modified *effective* Peclet number and dimensionless inlet temperature function. Finally, the accuracy of these predictions is evaluated by comparison to results of 3-D CFD modeling in Fluent, and design maps for optimizing the transient heating process are presented. Results indicate that the reduced-order models' simplicity, computational savings, and ability to capture the essential physics of the transient process justify their use in design calculations over more complex, highly detailed, numerical/CFD schemes.

Keywords: Solid oxide fuel cell; Thermal modeling; Transient analysis

1. Introduction

Solid oxide fuel cells (SOFCs) are currently being developed for mobile and stationary power plant applications, and much attention is being paid to the design and optimization of their steady state performance in an effort to make SOFC technology commercially viable in the near future. However, it is being increasingly realized [1] that because of substantial thermomechanical stresses developed in the cell components and stack, the transient process of heating an SOFC from room temperature to operating temperature (600–800 °C) during startup, or cooling down to ambient during shutdown must be given special attention as well. The ultra thin electrolyte and electrode layers (PEN structure) are prone to delamination, cracking, or other catastrophic failure if subjected to excessive thermal shock, temperature gradients, and thermal cycling during startup or shutdown processes.

These dangers can usually be avoided altogether by proceeding through the transient in a very slow, controlled fashion (in a recent ASME conference presentation Hawkes et al. [2] reported taking 2 days to bring a stack up to operating temperature). As SOFC technology matures, however, it is likely that the consumer will demand that the fuel cell reach operating conditions as quickly as possible, for example, in the cold start of an automobile [3]. Thus, the optimal design of a startup process will minimize the total time required for heating, subject to the constraint of some maximum allowable temperature gradient (to avoid thermomechanical fracture) as well as time rate of change of temperature (to avoid thermal shock and creep stresses). It will also be necessary to quantify the expected number of thermal cycles the cell can withstand during its lifetime, subject to the real possibility that faster heating times will lower the life expectancy of the cell.

In the literature, some preliminary efforts to address these concerns have been reported. Although numerous papers have presented the development of numerical/CFD models to simulate SOFC behavior at steady state, few are capable of simulating transient operation [1,3–5], and only one [1] has begun

* Corresponding author. Tel.: +1 404 385 1356; fax: +1 404 894 8496.
E-mail address: andrei.fedorov@me.gatech.edu (A.G. Fedorov).

0378-7753/$ – see front matter © 2005 Elsevier B.V. All rights reserved.
doi:10.1016/j.jpowsour.2005.11.072

Nomenclature

A	cross-sectional area of a cell component (m^2)
c_p	specific heat ($J\,kg^{-1}\,K^{-1}$)
h	convective heat transfer coefficient ($Wm^{-2}\,K^{-1}$)
k	thermal conductivity ($Wm^{-1}\,K^{-1}$)
K	rate of inlet temperature rise ($°C\,s^{-1}$)
K_{eff}	dimensionless (effective) rate of inlet temperature rise
L	length of channel (m)
Pe	effective Peclet number of the flow, $u_{eff}L/\alpha_{eff}$
T_f	final (operating) temperature (°C)
T_0	initial temperature (°C)
u	velocity of hot air stream ($m\,s^{-1}$)
u_{eff}	effective velocity of hot air stream ($m\,s^{-1}$)

Greek letters

α	thermal diffusivity ($m^2\,s^{-1}$)
α_{eff}	effective thermal diffusivity ($m^2\,s^{-1}$)
β_{eff}	parameter relating conduction to advection (m)
η	kinematic viscosity ($m^2\,s^{-1}$)
ρ	density ($kg\,m^{-3}$)
τ_c	advective time scale (s)
τ_h	total heating time (s)
τ_h^*	dimensionless total heating time
τ_i	inlet temperature function time scale (s)

to quantify thermally induced, transient thermal stresses during startup/shutdown. These models are based on finite element or volume approaches with the intent to give highly detailed information about current density, species distribution, flow and temperature fields, and propagation of thermal waves in the solid. Thus, the information required for transient design would be available, but the complexity of the models and the copiousness of the results may obscure the underlying physics of the process and prohibit the development of simple design rules for optimal transient heating/cooling processes (assuming such rules do exist). In addition, the rigorous CFD-based approaches demand a great deal of computational power, especially when simulating a long transient process with a large number of parameters to study. Adding to the computational expense is the very fine discretization required for numerical modeling because of the very high aspect ratio of components in the cell, for example, the 15 μm thick by 10 cm long electrolyte layer.

To overcome the above-mentioned conceptual and computational problems, we aim at developing reduced-order models and an analytical approach leading to the closed-form solution of the problem. Our ultimate goal is to develop simple, efficient design rules that clearly show the effects of the various system parameters on (1) the total time required for startup and (2) the maximum temperature gradients developed during the process. The interest is not in developing a model that can give a highly detailed prediction of the temperature field at any given moment in time, but rather, a model that accurately and efficiently predicts the *global* quantities just mentioned. This paper is the first to attempt to develop an efficient design strategy for optimizing the transient process and will focus on the initial startup of a cell from ambient temperatures with a simplified approach that generally (with few modifications) applies to shutdown as well.

2. Model formulation and approach

Under consideration is the planar type SOFC, which is a stack of repeating unit cells with dimensions shown in Fig. 1. The interconnects (current collectors) are made of stainless steel, the solid electrolyte is yttria-stabilized zirconia (YSZ), the porous anode is Ni-doped YSZ, and cathode is Sr-doped $LaMnO_3$ (LSM). The cell is heated by flowing hot air into the oxidizer channel while controlling the inlet air temperature as a function of time. As a first approximation, conditions in the fuel channel are assumed quiescent (negligible flow), with the composition of the gas phase similar to what would be found in a typical fuel stream. At startup, no electrochemical reactions take place until a prescribed temperature is reached, at which point electrochemical "light-off" occurs [6]. The electrochemical process generates heat, and consumes and produces chemical species in the flow streams, coupling the thermal-fluid model to the electrochemical model. For simplicity, it is assumed that a desired operating temperature is reached without triggering electrochemical reactions (i.e. no heat generation), so that attention is limited to convective heating of the cell.

Another simplifying assumption is that of a 1-D temperature field in each component of the cell, with variation only along the flow direction, as suggested by the high aspect ratio of the channel (>30:1). The small physical dimensions of the components also suggest that they may be in local thermal equilibrium (normal to the flow direction) and this possibility is investigated through the development and analysis of three reduced-order models of varying complexity. The first and most general model assumes the solid temperature is different from the gas temperature, and the resulting two-equation, coupled, transient model is solved numerically. The second model

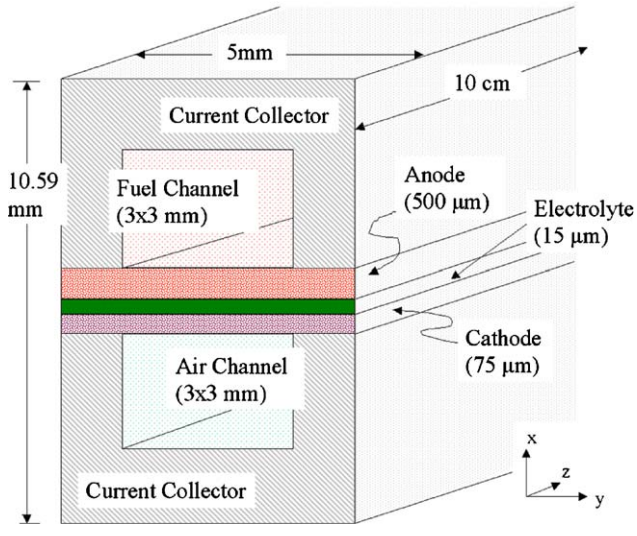

Fig. 1. Geometry of the unit cell of a planar type SOFC stack.

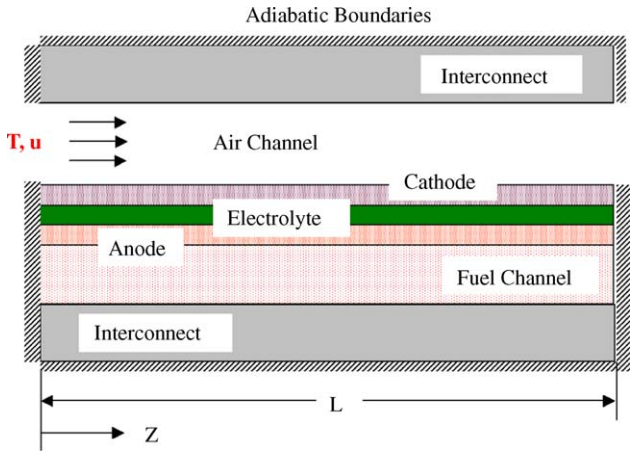

Fig. 2. Schematic of the unit cell as a channel with composite, insulated walls. The temperature profile is assumed 1-D in each layer with variation in the flow, z-direction only.

assumes the gas and solid are in local thermal equilibrium resulting in a single transient convective–conductive equation for which an analytical solution has been obtained [7]. The third model goes one step further in simplifying the problem and assumes that conduction along the flow direction is negligible compared to advection of thermal energy down the length of the cell. This latter model is thus a purely convective heating model, also yielding an analytical solution. The range of validity of these models is then established by comparing their predictions of heating time and maximum temperature gradients to the results of detailed, 3-D CFD simulations of SOFC unit cell. It is assumed that the geometry of the cell, material selection, and initial and final temperatures are prescribed design parameters, leaving the inlet air temperature and air velocity (flow rate) as parameters that can be used to optimize the heating process.

2.1. Two-equation, coupled, solid–gas model

The most general, reduced-order, transient heating model we developed is derived by applying conservation of energy to each layer (component) of the cell shown in Fig. 2. This yields a set of seven partial differential equations (PDEs) that are coupled through the temperature difference between adjoining layers. The equation for the air channel, assuming constant velocity plug flow and neglecting thermal radiation, is

$$(\rho c_p A)_g \left[\frac{\partial T_g}{\partial t} + u\frac{\partial T_g}{\partial z}\right] = (kA)_g \frac{\partial^2 T_g}{\partial z^2} - hP_{g\text{–}C}(T_g - T_C) - hP_{g\text{–}IC}(T_g - T_{IC}) \quad (1)$$

subject to the boundary and initial conditions

$$\text{BC's}: \quad T_g(0,t) = f(t); \quad \frac{\partial T_g}{\partial z}(L,t) = 0, \qquad \text{IC}: \quad T_g(z,0) = T \quad (2)$$

where h is the convective heat transfer coefficient, T_C and T_{IC} are temperatures of the cathode and interconnect, respectively, $P_{g\text{–}C}$ and $P_{g\text{–}IC}$ are the contact perimeters between the air (gas) channel and the cathode layer, and the air (gas) channel and the interconnect layer, respectively, A is the cross sectional area of the air channel, and k, ρ, c_p are the thermal conductivity, density, and specific heat of the air, respectively. Similar equations are written for the other layers, for example, the interconnect layer

$$(\rho c_p A)_{IC}\frac{\partial T_{IC}}{\partial t} = (kA)_{IC}\frac{\partial^2 T_{IC}}{\partial z^2} + hP_{g\text{–}IC}(T_g - T_{IC}) - \frac{P_{IC\text{–}C}}{R_{IC\text{–}C}}(T_{IC} - T_C) \quad (3)$$

which is coupled to the air equation through the convection term (the second term on the right-hand-side), and to the cathode layer (see Figs. 1 and 2) through the thermal resistance

$$R_{IC\text{–}C} = \frac{t_{IC}}{2k_{IC}} + \frac{t_C}{2k_C} \quad (4)$$

where, T_{IC}, t_C are the thickness of the interconnect and cathode layers, respectively. In like manner, the remaining equations for the cathode (C), electrolyte (E), anode (A), fuel channel (f), and lower interconnect (IC_2), are

$$(\rho c_p A)_C\frac{\partial T_C}{\partial t} = (kA)_C\frac{\partial^2 T_C}{\partial z^2} + hP_{g\text{–}C}(T_g - T_C) + \frac{P_{IC_1\text{–}C}}{R_{IC\text{–}C}}(T_{IC} - T_C) - \frac{P_{C\text{–}E}}{R_{C\text{–}E}}(T_C - T_E),$$

$$(\rho c_p A)_E\frac{\partial T_E}{\partial t} = (kA)_E\frac{\partial^2 T_E}{\partial z^2} + \frac{P_{C\text{–}E}}{R_{C\text{–}E}}(T_C - T_E) + \frac{P_{E\text{–}A}}{R_{E\text{–}A}}(T_E - T_A),$$

$$(\rho c_p A)_A\frac{\partial T_A}{\partial t} = (kA)_A\frac{\partial^2 T_A}{\partial z^2} + \frac{P_{E\text{–}A}}{R_{E\text{–}A}}(T_E - T_A) - hP_{f\text{–}A}(T_f - T_A) - \frac{P_{A\text{–}IC_2}}{R_{A\text{–}IC_2}}(T_A - T_{IC_2}),$$

$$(\rho c_p A)_{fuel}\frac{\partial T_{fuel}}{\partial t} = (kA)_{fuel}\frac{\partial^2 T_{fuel}}{\partial z^2} + hP_{f\text{–}A}(T_f - T_A) + hP_{f\text{–}IC_2}(T_f - T_{IC_2}),$$

$$(\rho c_p A)_{IC_2}\frac{\partial T_{IC_2}}{\partial t} = (kA)_{IC_2}\frac{\partial^2 T_{IC_2}}{\partial z^2} + \frac{P_{A\text{–}IC_2}}{R_{A\text{–}IC_2}}(T_A - T_{IC_2}) - hP_{f\text{–}IC_2}(T_f - T_{IC_2}) \quad (5)$$

The boundary and initial conditions for Eqs. (3) and (5) are all of the same form

$$\text{BC's}: \quad \frac{\partial T_i}{\partial z}(0,t) = \frac{\partial T_i}{\partial z}(L,t) = 0; \qquad \text{IC}: \quad T_i(z,0) = T_0 \quad (6)$$

Table 1
Material properties of cell components

Component	ρ (kg m^{-3})	k (W m^{-1} K^{-1})	c_p (J kg^{-1} K^{-1})
Anode (Ni-doped YSZ)	3030	5.84	595
Cathode (LSM)	3310	1.86	573
Electrolyte (YSZ)	5160	2.16	606
Current collector (SS)	8030	20.0	502
Air channel	0.58	0.047	1051
Fuel channel	0.2	0.2	5000

This set of coupled PDEs can be solved numerically in its current form, but a reasonable simplifying assumption at this point, is that the temperatures in the solid are locally uniform at each cross-section in the direction normal to the flow. This is verified by calculating the Biot number Bi, for this configuration as the ratio of thermal resistance across the entire composite channel wall, to convective thermal resistance between the channel walls and air stream

$$Bi = \frac{R_{\text{conduction}}}{R_{\text{convection}}} = h\sum_i \frac{t_i}{k_i} \tag{7}$$

where h is the convection heat transfer coefficient, t is the thickness of layer i and k is thermal conductivity. Using values found in Table 1 for k_i, dimensions from Fig. 1 for t_i, and estimating $h \sim 60\,\text{W m}^{-2}\,\text{K}^{-1}$ for fully-developed internal, laminar air flow in a 3 mm pipe, yields $Bi \sim 0.02$, validating the assumption that the solid can be treated as a locally isothermal lumped capacitance element. This understanding allows us to combine Eqs. (3) and (5) to formulate a single energy equation for the effective temperature of the solid matrix

$$\sum_i (\rho c_p A)_i \frac{\partial T_s}{\partial t} = \sum_i (kA)_i \frac{\partial^2 T_s}{\partial z^2} + h P_{g\text{–}s}(T_g - T_s) \tag{8}$$

with boundary and initial conditions

$$\text{BC's}: \quad \frac{\partial T_s}{\partial z}(0,t) = \frac{\partial T_s}{\partial z}(L,t) = 0; \qquad \text{IC}: \quad T_s(z,0) = T_0 \tag{9}$$

The equation for the gas is similar to Eq. (1)

$$(\rho c_p A)_g \left[\frac{\partial T_g}{\partial t} + u\frac{\partial T_g}{\partial z}\right] = (kA)_g \frac{\partial^2 T_g}{\partial z^2} + h P_{g\text{–}s}(T_s - T_g) \tag{10}$$

with the same boundary and initial conditions given in Eq. (2). We further consider the case when the inlet air temperature is defined by a linear increase in time until a desired final (T_f) steady-state temperature is reached

$$f(t) = \begin{cases} T_0 + Kt & t \le \dfrac{(T_f - T_0)}{K} \\ T_f & t > \dfrac{(T_f - T_0)}{K} \end{cases} \tag{11}$$

where K is the rate of temperature rise at the inlet in units of $^\circ\text{C s}^{-1}$. It should be noted that although the results for the linear temperature increase are discussed in this paper, all mathematical developments are general and could be readily extended in a straight-forward fashion to investigate any functional dependence of the inlet air temperature.

Eqs. (8) and (10) are solved numerically using a Crank–Nicholson, finite difference scheme [8]. The gas equation for the next future time step is solved by guessing a temperature distribution in the solid, and using the tri-diagonal matrix algorithm [8] to invert the coefficient matrix. Using this temperature distribution, the solid equation is solved in a similar manner, and the process repeated until the temperatures converge before proceeding to the next time step. The calculations proceed forward in time until steady-state is reached. Temperature gradients (spatial and temporal) are calculated numerically from the resulting temperature field history, allowing the maximum temperature gradients developed through the entire heating process to be identified. The only modification necessary for simulating cooling (rather than heating) processes is to use negative values for K in the boundary condition, Eq. (11).

2.2. Convective–conductive model

To further simplify Eqs. (8) and (10), and to enable closed-form analytical solution of the problem, an assumption of local thermal equilibrium between the gas and solid is employed. This bold simplification is applied to the problem at hand, not to prove or disprove that the solid and gas are at the same temperature, but to determine whether the approach will yield accurate predictions of heating time and maximum temperature gradients. If the model can accomplish this task, and do it analytically, then it is a very powerful design tool for optimizing the transient heating and cooling process.

To implement the local thermal equilibrium assumption correctly (i.e., without even locally violating energy conservation), the following procedure is employed: First, both conservation Eqs. (8) and (10) are added together, which cancels the coupling convective solid–gas heat exchange term. Then, by definition of local thermal equilibrium, the temperatures of the gas and solid are made the same, leading to the following single convective–conductive governing equation describing transient heating dynamics of the unit cell

$$\frac{\partial T}{\partial t} + u_{\text{eff}}\frac{\partial T}{\partial z} = \alpha_{\text{eff}}\frac{\partial^2 T}{\partial z^2} \tag{12}$$

where, u_{eff} is the *effective* velocity and α_{eff} is the *effective* thermal diffusivity defined as follows:

$$u_{\text{eff}} = \frac{(\rho c_p A)_g}{\sum_i (\rho c_p A)_i} u; \qquad \alpha_{\text{eff}} = \frac{\sum_i (kA)_i}{\sum_i (\rho c_p A)_i} \tag{13}$$

Note that the summations are now indexed to include every component of the cell including flow channels. The effective velocity is the physical air velocity scaled by the ratio of heat capacity of the air channel to energy stored in the channel walls. The

effective thermal diffusivity is the cross-sectional area-weighted diffusivity of the composite channel wall. Both of these terms are dominated by the relatively massive interconnects with their high conductivity, density, and cross-sectional area.

The same procedure used to derive Eq. (12) can be applied to the boundary and initial conditions (they must be first expressed in a conservative basis in terms of the total energy rate/flux [7]), yielding

$$\text{BC's}: \quad T(0,t) - \beta_{\text{eff}} \frac{\partial T}{\partial z}(0,t) = f(t);$$

$$\frac{\partial T}{\partial z}(L,t) = 0, \qquad \text{IC}: \quad T(z,0) = T_0 \tag{14}$$

where the coefficient β_{eff} in Eq. (14) combines thermal energy conduction in the solid to thermal energy transport in the air channel

$$\beta_{\text{eff}} = \frac{(kA)_{\text{IC}_1} + (kA)_{\text{C}} + (kA)_{\text{E}} + (kA)_{\text{A}} + (kA)_{\text{f}} + (kA)_{\text{IC}_2}}{(\rho c_{\text{p}} A)_{\text{g}} u} \tag{15}$$

Notice that if heat diffusion in the air is neglected – a very reasonable approximation as compared to advection – then, $\beta_{\text{eff}} = \alpha_{\text{eff}}/u_{\text{eff}}$.

When temperature, length, and time are normalized using the following characteristic scales:

$$T^* = \frac{T - T_0}{T_{\text{f}} - T_0}; \qquad z^* = \frac{z}{L}; \qquad t^* = \frac{t}{(L/u_{\text{eff}})} \tag{16}$$

the dimensionless form of Eq. (12) can be expressed as

$$\frac{\partial T^*}{\partial t^*} + \frac{\partial T^*}{\partial z^*} = \frac{1}{Pe} \frac{\partial^2 T^*}{\partial z^{*2}} \tag{17}$$

where Pe is defined as the *effective* Peclet number, $Pe = u_{\text{eff}} L/\alpha_{\text{eff}}$, that is, the ratio of advection of thermal energy down the length of the channel to diffusion of thermal energy in the solid layers of the SOFC unit cell. Likewise, the boundary and initial conditions are

$$\text{BC's}: \quad T^*(0,t^*) - \frac{1}{Pe} \frac{\partial T^*}{\partial z^*}(0,t^*) = F(t^*);$$

$$\frac{\partial T^*}{\partial z^*}(1,t^*) = 0, \qquad \text{IC}: \quad T^*(z^*,0) = 0 \tag{18}$$

where $F(t^*)$ is the non-dimensional form of the inlet temperature function given by Eq. (11)

$$F(t^*) = \frac{KL}{(T_{\text{f}} - T_0) u_{\text{eff}}} t^* \tag{19}$$

Eq. (19) reveals the second dimensionless parameter that determines the thermal response of the cell, the *effective* rate of inlet temperature rise

$$K_{\text{eff}} = \frac{L/u_{\text{eff}}}{(T_{\text{f}} - T_0)/K} \tag{20}$$

Physically, this parameter represents the ratio of the advective time scale, $\tau_{\text{c}} = L/u_{\text{eff}}$, to the time scale associated with the transient forcing of the inlet temperature, $\tau_{\text{i}} = (T_{\text{f}} - T_0)/K$ that is, the time required for the inlet air temperature to reach the final desired temperature. A significant insight into the transient heating process can be obtained by analyzing this parameter. In advection dominated flows ($Pe \gg 1$, note the modified definition of effective Peclet number here, combining properties of the air and solid), a value of K_{eff} greater than unity implies that the rate of thermal energy input at the inlet of the cell exceeds the capability of the cell to store and distribute this heat input. Thus, temperature at the inlet builds up too quickly, leading to excessive thermal gradients without significant improvement in total heating time.

The usefulness of Eq. (17) lies in the fact that an analytical series solution has been found [7] (see Appendix A for details), and that the temperature distribution dependence has been reduced to only two dimensionless parameters: effective Peclet number, Pe, and the effective rate of inlet temperature rise, K_{eff}. Also, this solution provides a convenient way to validate the numerical scheme used to solve Eqs. (8) and (10) in Section 2.1. As the heat transfer coefficient coupling the gas and solid temperatures is made arbitrarily large, the temperatures of the gas and solid should converge onto each other and the resulting single temperature solution must match the analytical result given by the closed-form solution of Eq. (17).

2.3. Purely convective model

A very interesting limiting case of Eq. (17) is that of purely convective flow ($Pe \to \infty$), in which case the right-hand side of Eq. (17) vanishes. The resulting equation

$$\frac{\partial T^*}{\partial t^*} + \frac{\partial T^*}{\partial z^*} = 0 \tag{21}$$

and in particular, its dimensional form

$$\frac{\partial T}{\partial t} + u_{\text{eff}} \frac{\partial T}{\partial z} = 0 \tag{22}$$

looks very much like the governing equation for a cell with thermally thin cell components (i.e. no thermal energy storage in cell components, and local thermal equilibrium between the solid and gas [7]). However, because the *effective*, not physical velocity is used here, thermal energy storage in the cell is properly accounted for, and only thermal energy conduction along the axial direction is neglected. The relevant boundary and initial conditions are, respectively

$$T^*(0,t^*) = F(t^*); \qquad T^*(z^*,0) = 0 \tag{23}$$

The method of characteristics yields the analytical solution of the time dependent, 1-D temperature distribution

$$T^*(z^*,t^*) = \begin{cases} 0, & z^* > t^* \\ K_{\text{eff}}(t^* - z^*), & z^* \le t^* \end{cases} \tag{24}$$

This very simple equation for the unsteady temperature distribution provides simple algebraic relationships for dimensionless heating time

$$\tau_h^* = \frac{1}{K_{\text{eff}}} + 1 \tag{25}$$

and dimensionless temperature gradients

$$-\left.\frac{\partial T^*}{\partial z^*}\right|_{\max} = \left.\frac{\partial T^*}{\partial t^*}\right|_{\max} = K_{\text{eff}} \tag{26}$$

The dimensional form of these equations yields some physical insight. The total heating time is the sum of the two time scales, τ_c and τ_i previously discussed in Section 2.2 above

$$\tau_h = \frac{T_f - T_0}{K} + \frac{L}{u_{\text{eff}}} \tag{27}$$

The fastest that the cell can be heated, assuming it is a perfect heat exchanger, is given by the time required to bring the incoming air to the desired operating temperature, plus the time required for thermal energy to travel from the inlet to the exit. So, Eq. (27) is the theoretical lower bound (minimum possible value) on heating time, and unambiguously suggests that heating time is inversely proportional to both K and u. The maximum dimensional (physical) temperature gradients become

$$-\left.\frac{\partial T}{\partial z}\right|_{\max} = \frac{K}{u_{\text{eff}}}; \qquad \left.\frac{\partial T}{\partial t}\right|_{\max} = K \tag{28}$$

indicating that spatial temperature gradient is inversely proportional to u, but both temperature gradients (spatial and temporal) increase linearly with K. Eq. (28) set upper bounds on the maximum temperature gradients that can exist in the solid during the transient heating, owing to the fact that thermal conduction, which tends to diminish temperature gradients, has been neglected in the formulation.

Eqs. (27) and (28) constitute very simple design rules that establish relationships between design parameters and clearly explain the competing effects that must be balanced to optimize the heating process

- Increasing flow velocity, u, tends to decrease both the heating time (*positive effect*) and spatial temperature gradient (*positive effect*), but has no effect on the temporal gradient.
- Increasing the rate of inlet temperature rise, K, tends to decrease the required heating time (*positive effect*), but increases both the temporal and spatial temperature gradients (*negative effect*).

Thus, the purely convective model has yielded useful information about limiting cases, which in hindsight seems to be almost intuitively obvious, and provides the framework for optimization of the heating process, even though the validity of the results still needs to be established. This is done in the next section. In order to determine whether or not the simple, reduced-order transient heating models have any significant bearing on reality, we compared their predictions of heating time and temperature gradients to the results of transient 3-D CFD simulations of SOFC unit cell heating.

2.4. CFD model

To critically compare the predictive power of the reduced-order transient thermal models, a fully three-dimensional thermal-fluid analysis of the unit cell in Fig. 1 was performed via the commercially available CFD software Fluent. In simulations, thermophysical properties of the solid materials were assumed constant (estimated at the average temperature) and are listed in Table 1. The steady-state flow field in the oxidizer channel was found under the assumption of laminar flow using constant thermophysical fluid properties evaluated at the average temperature of 300 °C. For simplicity, this flow field was then used for the unsteady calculations of the temperature field in the cell, as the inlet temperature was linearly increased from 25 to 625 °C. Once the inlet air temperature reached 625 °C, it was held constant until the normalized temperature of the solid at the end of the flow channel was within 5% of the normalized steady state value (i.e. 595 °C), at which point the simulations were terminated. The temperature history of the solid (electrolyte) was recorded throughout, and post-processed to yield maximum spatial and temporal temperature gradients. Because of symmetry along the axial midplane, only half of the unit cell was modeled using 44,000 discrete volumes. The mesh and time-step were properly refined to ensure that the results were mesh and time-step independent. The time-step for each simulation was adjusted based on the rate of inlet temperature rise, K, and typically corresponded to a 2 °C (per time step) temperature rise at the inlet.

Cases were run for K values of 0.01, 0.02, 0.05, 0.1, 0.2, 0.5, 1.0, and 2.0 °C s^{-1}. The inlet velocities used were, 1, 5, 10, and 20 m s^{-1}, corresponding to effective Peclet numbers of 0.8, 4.2, 8.4, and 16.7. Results of these simulations are compared with results of the reduced-order models in the next section.

3. Model results and analysis

First, the results of CFD simulations were compared to predictions obtained with the most general reduced-order model, which is the two-equation, coupled, solid–gas model described in Section 2.1. Before the two-equation model can be numerically solved, the heat transfer coefficient, h, must be specified at each point along the air channel. Because almost one-third of the channel is in the thermally-developing entrance region, the correlation based on the Graetz solution for thermally developing, hydrodynamically fully-developed laminar flow in a duct with constant wall temperature [9] was used to approximately account for variation in heat transfer coefficient along the channel length

$$Nu_x = 3.66 + \frac{0.0018}{x^{*1/3}(0.04 + x^{*2/3})^2}; \qquad x^* = \frac{x/D_h}{Re\ Pr} \tag{29}$$

where the Nusselt number at a given position, x, is $Nu_x = h_x D_h/k$, hydraulic diameter is $D_h = 4A_c/P_w$, the Reynolds number is $Re = uD_h/\eta$ and Prandtl number is $Pr = \eta/\alpha$.

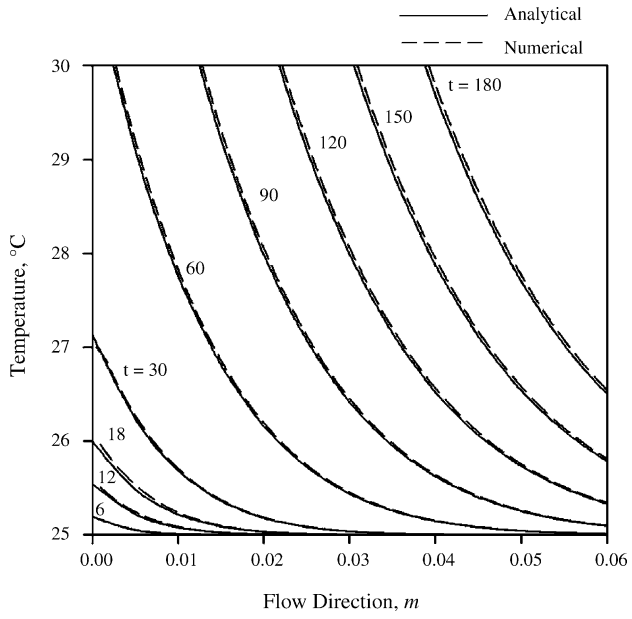

Fig. 3. Validation of numerical solution of two-equation, coupled solid–gas model (dashed line) vs. analytical solution of convective–conductive model (solid line) in the limit of local thermal equilibrium. The cell is in the initial stages of being heated by hot air with velocity, $u = 1\ \mathrm{m\,s^{-1}}$, and at a rate $K = 1\ ^\circ\mathrm{C\,s^{-1}}$. Simulation time (in seconds) for each temperature profile is indicated as a label for each curve in the figure.

Several steps were taken to validate the numerical solution of the two-equation, coupled, solid–gas model, Eqs. (8) and (10). First, the grid spacing was reduced until results were grid independent. This requirement was satisfied by discretizing the channel length into 100 nodes. Second, the time step was reduced until results were time-step independent, which occurred for the same time-step size as discussed in Section 2.4 for the CFD model. Finally, the numerical solution was validated against the analytical solution of the second reduced-order model in Section 2.3 in the limit of local thermal equilibrium. In order to force thermal equilibrium between the gas and solid, the heat transfer coefficient was made 1000 times larger than the baseline, thermally-fully developed value ($x^* \to \infty$) for laminar flow in a duct as predicted by Eq. (29). This caused the temperature difference between the gas and solid to vanish, and the resulting solid–gas temperature profile matched that obtained analytically by solving Eq. (12). Fig. 3 shows results of this validation test for a cell in the initial stages of being heated by air flowing at $u = 1\ \mathrm{m\,s^{-1}}$ with the inlet air temperature increasing at a rate of $K = 1\ ^\circ\mathrm{C\,s^{-1}}$. The analytical and numerical solutions match very well for this case as well as several other cases that were run, thus establishing the validity of the numerical procedure used for integration of the 1st reduced-order model, Eqs. (8) and (10).

Having validated the numerical scheme for solving the two-equation coupled, solid–gas model, the predictions of heating time and maximum temperature gradient were compared to the results of the CFD Fluent simulations. Figs. 4 and 5 show heating time, spatial temperature gradient, and temporal temperature gradient vs. rate of inlet temperature rise, K, for a heating air velocity of $u = 10\ \mathrm{m\,s^{-1}}$. The predictions of heating time and temporal temperature gradient show excellent agreement

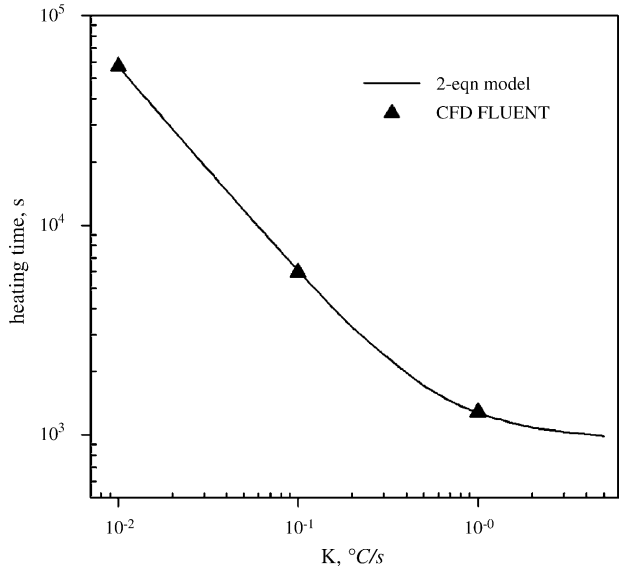

Fig. 4. Predictions of heating time vs. K for hot air velocity, $u = 10\ \mathrm{m\,s^{-1}}$. The solid line is the two-equation, coupled, solid–gas model predictions, and the triangles are data points obtained from 3-D CFD Fluent simulations.

for a wide range of K. However, the model significantly over predicts spatial temperature gradients (>100% error) as seen in Fig. 5. In fact, this was seen to be the case for most values of u that were used in simulations. Further investigation revealed that the excessive temperature gradients occurred near the inlet and were highly sensitive to the assumed behavior of

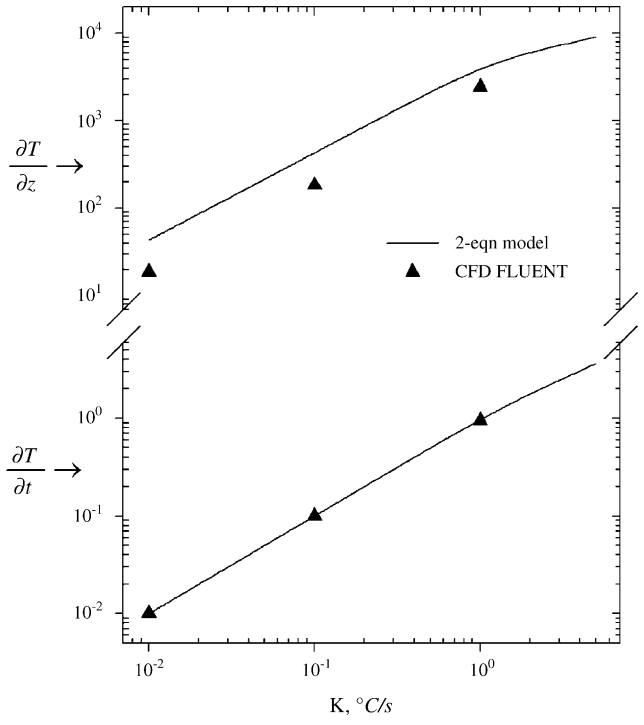

Fig. 5. Predictions of maximum temperature gradient vs. K for hot air velocity, $u = 10\ \mathrm{m\,s^{-1}}$. The solid line is the two-equation, coupled, solid–gas model predictions, and the triangles are results of 3-D CFD Fluent simulations. The upper plot is for spatial temperature gradient and the lower plot is for temporal temperature gradient.

heat transfer coefficient, h, which increases dramatically near the inlet. Indeed, the constant-wall temperature correlation, Eq. (29), appeared to predict significantly larger values of h (near the inlet) than what was found by rigorous solution of the conjugate mass, momentum, and energy conservation equations in the Fluent CFD model. In reality, h varies with air velocity, distance from the inlet, thermal condition of the channel walls, and time, a relationship not explicitly known, and requiring solution of a much more complicated conjugate heat transfer problem (see for example, [10,11]). Adding this significant additional level of complexity to the two-equation coupled solid–gas model would cut into its expected advantage of being much simpler and more computationally efficient than the 3-D Fluent model.

Having established that the two-equation coupled solid–gas numerical model is severely limited in its ability to be used as a reliable transient process design tool for SOFCs, the remainder of this paper will focus on the analytical model results and their application to optimal design of SOFC transient heating process. These two analytical reduced-order models – for purely convective and convective–conductive heating – were solved for a range of realistic values of effective rate of inlet temperature rise, K_{eff}, and effective Peclet number, Pe. All calculations were performed for the SOFC geometry shown in Fig. 1 and the material property values given in Table 1. The studied values of Pe correspond to physical velocity in the range $1 \le u \le 20\,\text{m s}^{-1}$, and the values of K_{eff} covers the range $0.01 \le K \le 5\,^{\circ}\text{C s}^{-1}$ in terms of the actual rate K of the inlet air temperature rise. Model predictions of dimensionless heating time, and maximum temperature gradients (spatial and temporal) are shown in Figs. 6–8. Strictly speaking, the purely convective model is the limiting case of the convective–conductive model, in the limit of $Pe \to \infty$. However, the convective–conductive model results rapidly converge to the purely convective model results for effective Peclet numbers as small as 10. Thus, the results for the case of $Pe = 16.7$ shown in the plots are obtained using the purely convective model calculations with the realization that further increases in Pe do not change the behavior.

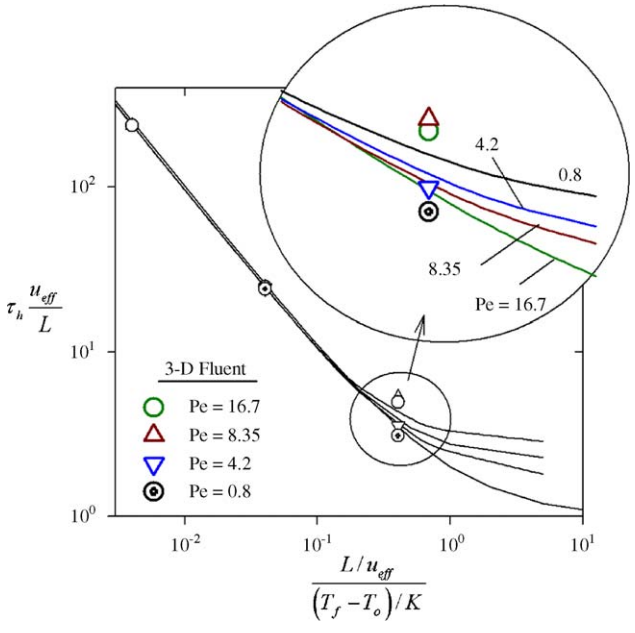

Fig. 6. Dimensionless heating time, τ_h^*, as a function of K_{eff} for various effective Peclet numbers. The solid lines are the reduced-order analytical model predictions and the data points are results of 3-D Fluent simulations. For $K_{\text{eff}} \ll 1$ the analytical models (regardless of Peclet number) accurately predict heating time. As K_{eff} increases, the analytical models are less accurate but still predict the correct trend. For large Peclet numbers (e.g. $Pe = 16.7$) both analytical models (i.e., for purely convective and convective–conductive heating) predict identical results.

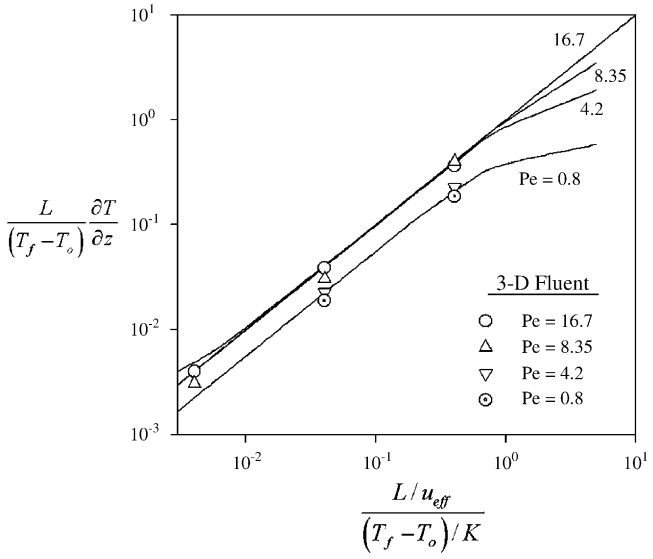

Fig. 7. Maximum dimensionless spatial temperature gradient as a function of K_{eff} for various Peclet numbers. The solid lines are the analytical convective–conductive model predictions and the data points are results of 3-D Fluent simulations. Temperature gradients decrease with a decrease in Pe at a fixed K_{eff}. The case of $Pe = 16.7$ is as calculated from the purely convective model (the limiting case of $\text{Pe} \to \infty$), which yields results identical to those obtained using the convective–conductive model at such a high Peclet number.

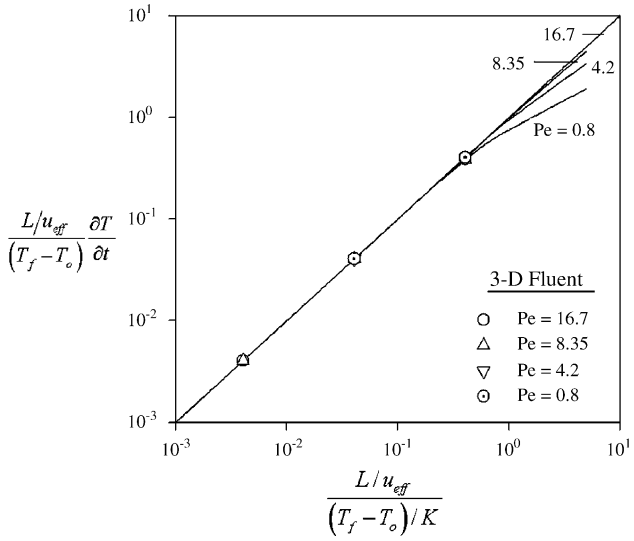

Fig. 8. Maximum dimensionless temporal temperature gradient as a function of K_{eff} for various Peclet numbers. The solid lines are the analytical model predictions and the data points are results of 3-D Fluent simulations. Excellent agreement between the analytical models and 3-D results is observed across a wide range of K_{eff}. At values of $K_{\text{eff}} < \sim 0.5$ the Peclet dependence is negligible and the purely convective heating analytical model provides satisfactory results.

3.1. Heating time

The first quantity of interest in transient thermal modeling of SOFCs is the total time required to heat the cell to the desired operating temperature. Fig. 6 shows total dimensionless heating time for various K_{eff}. The dimensionless heating time predicted by the purely convective reduced-order model is simply $\tau_{\text{h}}^{*} = 1/K_{\text{eff}} + 1$, which is a much 'nicer' result than the infinite series solution of the convective–conductive model. However, it is apparent from Fig. 6 that the convective–conductive model and the purely convective model give virtually indistinguishable results for any (even small) *Pe* as long as K_{eff} is sufficiently small. At larger K_{eff}, some *Pe* dependence is seen, with heating time asymptotically approaching a finite value (dimensionless value greater than 1) depending on *Pe*. Another feature of Fig. 6 is that excellent agreement (<2% error) is obtained between the analytical models and 3-D Fluent simulation results at small values of effective rate of inlet temperature rise, $K_{\text{eff}} \sim <0.1$. This lack of *Pe* dependence and good agreement with rigorous CFD simulations is hardly surprising when considered in the context of the physical time scales, τ_{c} and τ_{i}, identified in Section 2.2 of this paper. Small K_{eff} implies that the time scale associated with the prescribed rate of inlet temperature rise, $\tau_{\text{i}} = (T_{\text{f}} - T_0)/K$, is primarily responsible for determining how fast the cell can be heated. Thus, with respect to predictions of total heating time, the details of heat transfer within the cell are practically irrelevant! (The relevant portion of the analysis was implicitly included in the statement that K_{eff} is small.) For large K_{eff} this is no longer the case; the time scale (and mechanism) for heat flow within the channel (whether by advection or conduction) is of critical importance, and a rigorous multi-dimensional thermal-fluid analysis is required in order to accurately predict heating time. Fortunately, K_{eff} (as related to SOFC unit cells) is often small, and use of the purely convective model for prediction of heating time is quite accurate for practical purposes.

3.2. Maximum spatial temperature gradient

The second quantity of interest in transient thermal modeling of SOFCs is maximum spatial temperature gradient, which sets an upper limit on thermomechanical stress developed in the cell during its transient heating. The purely convective model prediction of dimensionless maximum temperature gradient is explicitly stated in Eq. (28). On the other hand, convective–conductive model predictions of temperature gradient were calculated numerically from the analytical solution of Eq. (17). Results of these two models along with predictions obtained using the 3-D Fluent simulations are shown in Fig. 7. Satisfactory agreement between the models (<20% error) is seen at high effective Peclet numbers ($Pe \geq 8$) for $K_{\text{eff}} \sim <1$. It is clear that the purely convective model over predicts temperature gradients for very low *Pe*, although it still predicts the correct trends. The convective–conductive model provides some improvement at very low *Pe*, but it is not reliable for intermediate values. An expected, yet interesting feature of the graphs shown in Fig. 7 is that the dimensionless temperature gradient for any given K_{eff} decreases with a decrease in *Pe* from its maximum at large *Pe* values (purely convective model). This is due to the fact that the addition of conduction as a significant heat transfer mechanism reduces temperature gradients along the axial direction. This does not imply, however, that real (physical) temperature gradients decrease with a decrease in velocity. The only way that lowering the effective Peclet number will result in lower (real) temperature gradients is by increasing the effective thermal diffusivity of the cell. Unfortunately, this may not be a viable design option, as it requires changing the geometry of the cell or selecting new materials, which are usually optimized for the most efficient steady-state operation.

3.3. Maximum temporal temperature gradient

One last quantity of interest in transient operation of a cell is the maximum temporal temperature gradient in cell materials. This is important because the cell is composed of layers made of different materials with different thermal expansion coefficients and characteristic time scales for creep. If the temporal temperature gradient exceeds the rate at which creep can relax interfacial stress due to thermal expansion mismatch, then delamination, cracking, or other failure may occur. Fig. 8 is a plot of the maximum dimensionless temporal temperature gradient for various *Pe* and K_{eff}. Clearly, for the values of K_{eff} less than ~1, the temporal gradient is essentially independent of *Pe*, showing excellent agreement with the 3-D Fluent model results. Thus, results given by the purely convective heating model are valid for prediction of the local rate of temperature change during transient heating of the SOFC.

For the three global quantities of interest-heating time, maximum spatial temperature gradient, and maximum temporal temperature gradient, we find then, that the purely convective model provides satisfactory results within certain limits of parameters. For heating time predictions, the model is valid for $K_{\text{eff}} \leq 0.1$ and $1 \leq Pe \leq \infty$. The purely convective model may be valid at even smaller effective Peclet numbers, but we do not have data to support this, and do not envision scenarios in which such low *Pe* is a realistic operating regime. For maximum spatial temperature gradients, the model is reasonably accurate for $K_{\text{eff}} \leq 1$ and $5 \leq Pe \leq \infty$. If in-depth, precise local information, beyond simply the maximum temperature gradient, is required, we recommend multi-dimensional, CFD modeling such as that described in Section 2.4. The purely convective heating model is also valid for predicting maximum temporal temperature gradients in the ranges $K_{\text{eff}} \leq 1$and $1 \leq Pe \leq \infty$. Because the convective–conductive model provides little improvement for expanding this range of validity, we recommend a design procedure for the heating/cooling process based on the purely convective model only. Note that this model is shown to have good predictive capabilities for the global heating/cooling characteristics just mentioned, and not necessarily for giving detailed time-varying temperature fields within the cell.

4. Design maps for transient SOFC heating and cooling

Figs. 6–8 are design maps, which can be used to develop a protocol for an optimal SOFC heating process. Typically,

the cell geometry and material selection will be optimized for steady-state cell performance, leaving the hot air velocity, u, and heating rate, K, as control variables for optimizing the transient process. Assuming that the maximum allowable stress (and corresponding temperature gradient) has been specified through a thermo-mechanical stress analysis of the unit cell, the design goal is to minimize heating time through proper choice of K and u. Because of the use of properly scaled dimensionless variables, Figs. 6–8 have the advantage of presenting a large amount of information on a single curve. A detailed, step-by-step design procedure based on similar maps has been presented by Damm and Fedorov [7]. Here, however, it is advantageous to refer back to physical parameters in outlining a design procedure for optimization of the heating/cooling process.

In particular, Fig. 9 shows a design map created from the purely convective model predictions (see Eqs. (27) and (28)). This model was shown in Section 3 to be valid over specific ranges of effective Peclet number and effective rate of inlet temperature rise. The map in Fig. 9 is specific to the geometry and material selection previously specified (see Fig. 1 and Table 1), and considers a unit cell being heated from 25 to 625 °C (the map is applicable for any process involving a 600 °C temperature change). Lines of constant K and u are shown with maximum spatial temperature gradient on the vertical axis and heating time on the horizontal axis. Once a horizontal line corresponding to the maximum allowable temperature gradient is specified, K and u can be chosen below that line such that heating time is minimized. This allows some flexibility in choice of K and u but these parameters are likely to be restricted by system constraints such as pumping power, heater size, etc. Alternatively, the maximum allowable heating time could be the specified design constraint, in which case K and u are chosen such that temperature gradient is minimized. This would give an estimate of the allowable gradients that the cell must be designed to withstand if the heating time requirement is to be met. Notice that increasing the air flow speed, u, always allows movement in a favorable direction on the map (i.e., reduction in both the heating time and maximum temperature gradients), while increasing K yields the mixed result of lowered heating time but increased temperature gradients. A design map such as Fig. 9 is thus an excellent graphical representation of how the design space may be efficiently searched to yield approximate values of hot air velocity and heating rate to achieve an optimal design of SOFC transient heating process. Fig. 9 is equally valid for heating and cooling of the cell; however, the maximum allowable temperature gradient for a heating process may be different than that for cell cooling due to differences in thermomechanical material behavior under heating and cooling conditions. Once the parameter K and u values resulting in optimal transient operation have been obtained, only a minimal amount of highly-intensive CFD computations can be used to yield the detailed information required to complete a thermo-mechanical failure analysis of the cell.

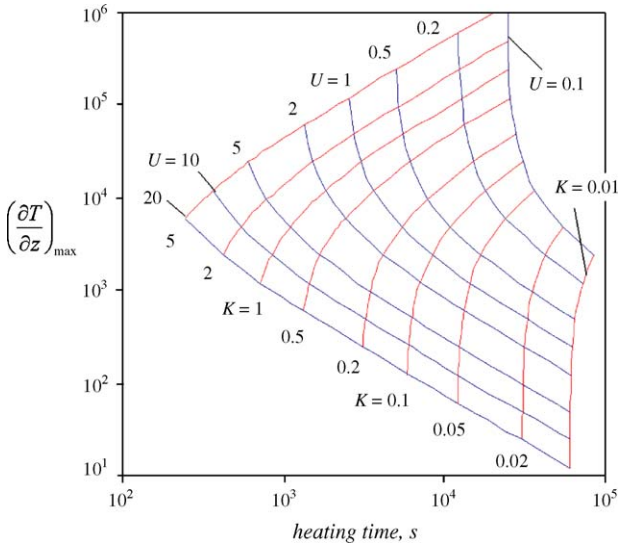

Fig. 9. Design map based on purely convective model predictions of spatial temperature gradient (°C m^{-1}) vs. heating time (s) for various K and u. This map is specific to the cell geometry and materials described in Fig. 1 and Table 1, and is applicable to a cell being heated or cooled over a 600 °C temperature interval.

5. Conclusions and future work

Reduced-order transient thermal models of varying complexity have been considered for optimizing the heating and cooling of an SOFC unit cell. The first and most general one, the two-equation, coupled solid–gas model resulted in fast numerical solution of the problem, compared to CFD simulations, but was shown to be unreliable for predicting maximum temperature gradients. The next two models the convective–conductive heating and purely convective heating permitted analytical solutions of the time-varying temperature field in the cell. The simplest of these, the purely convective heating model, also yielded explicit, algebraic relationships between heating time, temperature gradients, hot air velocity, and heating rate. These predictions of integral thermal quantities (i.e., the heating time and maximum spatial and temporal temperature gradients) were shown to be valid for a fairly broad range of operating parameters through comparison with fully 3-D Fluent simulations. The more general convective–conductive model of the cell provided little improvement in accuracy over the purely convective model; however, its formulation and analysis led to the definition of the appropriate scales for physical velocity and the dimensionless parameters that govern cell transient response.

Predictions of the analytical models have been presented in the form of generalized thermal design maps, and a specific example of a design map based on the purely convective model was used to develop a conceptual framework for optimizing a heating and cooling process. Our analysis shows that increasing the velocity of the hot air stream, and lowering the Peclet number (by increasing the effective thermal diffusivity of the cell) leads to the optimal design, which minimizes heating time under the constraint of maximum allowable temperature gradients. While this result is hardly surprising in hindsight, the ability of the purely convective model to accurately predict favorable design trends with little or no computational effort makes it a powerful tool for searching the design space in the early stages of transient process development.

Throughout the development of these reduced-order models and thermal design maps, it has been assumed that the maximum allowable temperature gradient (to avoid failure of cell components) is known a priori based on thermo-mechanical stress analysis. This is not necessarily the case and efforts similar to [1] are required for the development of relationships between failure, maximum allowable stresses, and maximum allowable temperature gradients as relevant to SOFC transients. Also, the effects of thermal cycling require additional research, in particular quantification of cell lifetime in terms of number of cycles and maximum temperature gradients developed during each cycle.

Another assumption of the current analysis that will be challenged is that the cell is perfectly insulated. In reality, the cell heat losses are temperature dependent (increasing as the cell heats up), which raises the possibility that the heating times could be much longer than what has been predicted here. In the most extreme case, a cell might never reach the desired operating temperature if the magnitude of heat input is not sufficiently larger than heat losses. The assumption of negligible flow in the fuel channel may also come into question depending on the flow rate of a reducing gas to keep the anode from oxidation at elevated temperatures (i.e. $T \geq 400\,^{\circ}\mathrm{C}$). To account for this, the energy conservation equation for the fuel channel in the system of Eqs. (5) and associated boundary/inlet condition would have to be modified to include an advective term. As a result, the two-equation model (Section 2.1) would become a three-equation model. This extension is straight-forward and follows the general theoretical framework we have outlined. Alternatively, the heat losses due to the flowing reducing gas on the anode side can be included into the two-equation and single equation models by using an ad-hoc approach through specifying a semi-empirical heat loss term along the unit cell length. In either case, the treatment is highly case-specific, so we refrain from its detailed consideration in presenting the results of a more general nature. Finally, extension and validation of the current analysis for other geometries, such as cross-flow cells, will greatly expand the applicability of the results. This future work will complement and enhance the presently developed simple and computationally efficient design rules for transient heating/cooling of the SOFC.

Acknowledgements

The support of this work by DOE through the Phase II SECA program, and DoD through the NDSEG fellowship program is acknowledged and appreciated.

Appendix A. Analytical solution of convective–conductive Eq. (17)

We seek a solution of the dimensionless governing Eq. (17) (*superscript has been dropped for clarity)

$$\frac{\partial T}{\partial t} + \frac{\partial T}{\partial z} = \frac{1}{Pe}\frac{\partial^2 T}{\partial z^2} \tag{30}$$

subject to the boundary and initial conditions

$$T(0,t) - \frac{1}{Pe}\frac{\partial T}{\partial z}(0,t) = F(t); \quad \left.\frac{\delta T}{\delta z}\right|_{z=1} = 0, \qquad T(z,0) = 0 \tag{31}$$

Look for a solution of the form

$$T(z,t) = \theta(z,t)\,\mathrm{e}^{Az+Bt} \tag{32}$$

where A and B are arbitrary constants. It can be shown that if $A = Pe/2$ and $\mathrm{B} = Pe/4$ then the advection term in Eq. (30) vanishes, yielding

$$\frac{\partial \theta}{\partial t} = \frac{1}{Pe}\frac{\partial^2 \theta}{\partial z^2} \tag{33}$$

where the dimensionless inlet forcing function from Eq. (31) becomes

$$Pe\,F(t)\,\mathrm{e}^{-Bt} = f(t) \tag{34}$$

The new problem can be expressed as

$$\theta(z,t) = \theta^{*}(z,t) + D_1(t)z + D_2(t) \tag{35}$$

where the unknown functions are selected such that the boundary conditions become homogeneous yielding

$$\theta(z,t) = \theta^{*}(z,t) + \frac{4 + 2Pe - 2Pe\,z}{Pe(4+Pe)} f(t) \tag{36}$$

The new problem to be solved is

$$\frac{\partial \theta^{*}}{\partial t} = \frac{1}{Pe}\left[\frac{\partial \theta^{*}}{\partial z^2} - S(z,t)\right]; \quad \text{where,}$$
$$S(z,t) = \frac{4 + 2Pe - 2Pe\,z}{(4+Pe)} f'(t) \tag{37}$$

which can now be solved analytically. The homogeneous portion of Eq. (37) is solved using separation of variables and the complete solution is assumed a Fourier series expansion based on the complete eigenvector set of the homogeneous problem but with time varying coefficients $C_n(t)$

$$\theta^{*}(z,t) = \sum_{n=1}^{\infty} C_n(t)\left[\sin(\omega_n z) + \frac{2\omega_n}{Pe}\cos(\omega_n z)\right] \tag{38}$$

where

$$C_n(t) = \frac{\int_0^1 \theta^{*}(z,t)\left[\sin(\omega_n z) + (2\omega_n/Pe)\cos(\omega_n z)\right]\mathrm{d}z}{\int_0^1 \left[\sin(\omega_n z) + (2\omega_n/Pe)\cos(\omega_n z)\right]^2 \mathrm{d}z} \tag{39}$$

The denominator is the squared eigenvector norm, which we will call G_n for simplicity

$$G_n = \frac{1}{2\omega_n Pe^2}\left[\left(2\omega_n^2 - \frac{1}{2}Pe^2\right)\sin*(2\omega_n) - 2\omega_n Pe\,(\cos(2\omega_n) - 1) + 4\omega_n^3 + Pe^2\omega_n\right] \quad (40)$$

with the eigenvalues $\omega_n = \lambda_n\sqrt{Pe}$ satisfying the following characteristic equation:

$$\cos(\omega_n) + \frac{Pe^2 - 4\omega_n^2}{4\omega_n Pe}\sin(\omega_n) = 0 \quad (41)$$

It follows, after some manipulation [7]:

$$C_n(t) = -e^{-\lambda_n^2 t}\frac{1}{G_n Pe}\int_0^t e^{\lambda_n^2\tau}\int_0^1 S(z,\tau) \times \left[\sin(\omega_n z) + \frac{2\omega_n}{Pe}\cos(\omega_n z)\right] dz d\tau$$

After applying the inlet temperature function from Eq. (11) and carrying out the integration, $C_n(t)$ is

$$C_n(t) = \frac{2K_{\text{eff}}}{G_n\omega(4\lambda_n^2 + Pe)^2} \times \left[(16\lambda_n^2 + Pe^2 t + 4Pe\lambda_n^2 t)\,e^{(Pe/4)t} - 16\lambda_n^2\,e^{-\lambda_n^2 t}\right] \quad (42)$$

Finally, $C_n(t)$ for the final, constant portion of the inlet temperature function (see Eq. (11)) is found to be

$$C_n(t) = -\frac{2Pe}{\omega G_n(4\lambda_n^2 + Pe)}\left[e^{(Pe/4)t} - e^{\lambda_n^2(t_1 - t) + (Pe/4)t_1}\right] \quad (43)$$

where $t_1 = 1/K_{\text{eff}}$ is the simulation time after which the inlet temperature is held constant.

References

[1] A. Selimovic, M. Kemm, T. Torisson, M. Assadi, J. Power Sources 145 (2005) 463–469.
[2] G. Hawkes, J. O'Brien, C. Stoots, S. Herring, M. Shahnam, in: Proceedings of the HT2005 ASME Summer Heat Transfer Conference, San Francisco, CA, 17–22 July 2005.
[3] L. Petruzzi, S. Cocchi, F. Fineschi, J. Power Sources 118 (2003) 96–107.
[4] M.A. Khaleel, Z. Lin, P. Singh, W. Surdoval, D. Collins, J. Power Sources 130 (2004) 136–148.
[5] W.A. Rogers, R.S. Gemmen, C. Johnson, M. Prinkey, M. Shahnam, in: Proceedings of the Fuel Cell Science Engineering Technology, ASME, Rochester, NY, 2003, pp. 517–520.
[6] C.L. Haynes, J.C. Ford, in: Proceedings of the HT2005 ASME Summer Heat Transfer Conference, San Francisco, CA, 17–22 July 2005.
[7] D.L. Damm, A.G. Fedorov, in: Proceedings of the HT2005 ASME Summer Heat Transfer Conference, San Francisco, CA, 17–22 July 2005.
[8] W.H. Press, S.A. Teukolsky, W.T. Vetterling, B.P. Flannery, Numerical Recipes in C, 2nd ed., Cambridge University Press, New York, 1995.
[9] S. Kakac, R.K. Shah, W. Aung, Handbook of Single-phase Convective Heat Transfer, Wiley and Sons, New York, 1987.
[10] J. Sucec, J. Heat Transf. 109 (1987) 295–299.
[11] A.G. Fedorov, R. Viskanta, Int. J. Heat Mass Transf. 43 (2000) 399–415.